



**HAL**  
open science

## Parent beta grain reconstruction of globularized Ti-6Al-4V alloy

Qian Wang, Margaux Saint Jalme, Christophe Schuman, Jean-Sébastien Lecomte, Christophe Desrayaud, Julien Favre, D. Fabrègue, Sylvain Dancette, Florian Mercier, Etienne Archaud, et al.

### ► To cite this version:

Qian Wang, Margaux Saint Jalme, Christophe Schuman, Jean-Sébastien Lecomte, Christophe Desrayaud, et al.. Parent beta grain reconstruction of globularized Ti-6Al-4V alloy. *Materials & Design*, 2021, pp.110280. 10.1016/j.matdes.2021.110280 . hal-03446979

**HAL Id: hal-03446979**

**<https://hal.science/hal-03446979>**

Submitted on 26 Sep 2022

**HAL** is a multi-disciplinary open access archive for the deposit and dissemination of scientific research documents, whether they are published or not. The documents may come from teaching and research institutions in France or abroad, or from public or private research centers.

L'archive ouverte pluridisciplinaire **HAL**, est destinée au dépôt et à la diffusion de documents scientifiques de niveau recherche, publiés ou non, émanant des établissements d'enseignement et de recherche français ou étrangers, des laboratoires publics ou privés.



## Parent beta grain reconstruction of globularized Ti-6Al-4V alloy

Qian Wang<sup>a,b,\*</sup>, Margaux Saint Jalme<sup>c,d</sup>, Christophe Schuman<sup>a,b,\*</sup>, Jean-Sébastien Lecomte<sup>a,b,\*</sup>,  
Christophe Desrayaud<sup>c</sup>, Julien Favre<sup>c</sup>, Damien Fabrègue<sup>d</sup>, Sylvain Dancette<sup>d</sup>, Florian Mercier<sup>d</sup>,  
Etienne Archaud<sup>e</sup>, Christian Dumont<sup>e</sup>



<sup>a</sup> Laboratoire d'Etude des Microstructures et de Mécanique des Matériaux (LEM3), Université de Lorraine, CNRS, Arts et Métiers ParisTech, 57073 Metz, France

<sup>b</sup> Laboratory of Excellence on Design of Alloy Metals for Low-mAss Structures (DAMAS), Université de Lorraine, 57073 Metz, France

<sup>c</sup> Mines Saint-Etienne, Univ Lyon, CNRS, UMR 5307 LGF, Centre SMS, 42023 Saint-Etienne, France

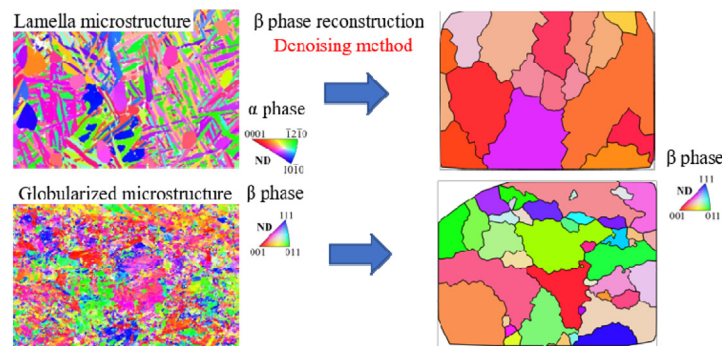
<sup>d</sup> Univ Lyon, INSA Lyon, CNRS UMR5510, Laboratoire MATEIS, 69621 Villeurbanne Cedex, France

<sup>e</sup> Aubert & Duval, R&D Department, BP 1, 63770 Les Ancizes, France

### HIGHLIGHTS

- A new  $\beta$  reconstruction method by filling restrained  $\beta$  phase with denoising technique.
- The reconstruction method is suitable for both lamellar and globularized  $\alpha$  microstructures.
- Multi-axial hot compression can achieve well globularization microstructure.

### GRAPHICAL ABSTRACT



### ARTICLE INFO

#### Article history:

Received 22 September 2021

Revised 7 November 2021

Accepted 23 November 2021

Available online 23 November 2021

#### Keywords:

Ti-6Al-4V

$\beta$  phase reconstruction

Multi-axial hot compression

Globularization

Recrystallization

### ABSTRACT

In this study, a denoising method of smoothing spline is proposed to reconstruct parent  $\beta$  grain of titanium alloys as a supplement to the past literatures. The  $\beta$  mean orientation of the sample with bimodal microstructure can be well reconstructed with similar grain size and negligible misorientation ( $<1^\circ$ ) compared with traditional reconstruction result. The second test case deals with globularized  $\alpha$  grains after multi-axial hot compression. Obvious  $\beta$  recrystallization happens inside the large prior  $\beta$  grain during deformation, which can facilitate the homogeneous globularization process. The mean orientation reconstruction of recrystallized  $\beta$  grain by smoothing spline is performed and further compared with the orientation calculated from one  $\alpha$  colony by orientation-trace method. The maximum  $20^\circ$  misorientation exists due to the local orientation deviation inside both  $\alpha$  and  $\beta$  grains during globularization processing. In addition, the globularization mechanism under multi-axial hot compression is analyzed. Despite the appearance of local heterogeneity between different  $\alpha$  colonies, high globularized efficiency around 71.2% can be easily achieved by the multi-directional deformation.

© 2021 Published by Elsevier Ltd. This is an open access article under the CC BY-NC-ND license (<http://creativecommons.org/licenses/by-nc-nd/4.0/>).

\* Corresponding authors at: Laboratoire d'Etude des Microstructures et de Mécanique des Matériaux (LEM3), Université de Lorraine, CNRS, Arts et Métiers ParisTech, 57073 Metz, France.

E-mail addresses: [qian.wang@univ-lorraine.fr](mailto:qian.wang@univ-lorraine.fr) (Q. Wang), [christophe.schuman@univ-lorraine.fr](mailto:christophe.schuman@univ-lorraine.fr) (C. Schuman), [jean-sebastien.lecomte@univ-lorraine.fr](mailto:jean-sebastien.lecomte@univ-lorraine.fr) (J.-S. Lecomte).

<https://doi.org/10.1016/j.matdes.2021.110280>

0264-1275/© 2021 Published by Elsevier Ltd.

This is an open access article under the CC BY-NC-ND license (<http://creativecommons.org/licenses/by-nc-nd/4.0/>).

### 1. Introduction

Titanium alloys, especially two – phases Ti-6Al-4V, offer a range of combinations of strength, toughness and high temperature

properties (e.g. superplasticity) that make them attractive in wide ranging aerospace and chemical industries [1]. It is usually processed by hot forging involving series of plastic deformations followed by rotations. Indeed, thermomechanical processing is the most common method to break down the lamellar microstructure of  $\alpha$  phase (known as globularization) and achieve favorable mechanical properties of Ti-6Al-4V. An new experimental method proposed in [2] includes multiaxial forging combined with heterogeneous temperature and intermediate delay between deformation steps, which offers the opportunity to get closer to industrial open die forging conditions. The well globularization microstructure obtained by the above method will be involved in this work.

$\beta$  phase can influence the dominant deformation mechanism of Ti alloy during hot working, because it is considerably softer than  $\alpha$  during hot working with higher diffusivity and more active slip systems [3]. When the volume fraction of  $\beta$  is large enough at high temperature (>850 °C), the grain boundary sliding can be accommodated by the deformation of  $\beta$  instead of  $\alpha$  phase [4]. The formation of subgrain and dynamic recrystallization in  $\alpha$  occurs when the  $\beta$  volume fraction is lower at a temperature lower than 850 °C.  $\beta$  phase plays an important role in the deformation compatibility between  $\alpha$  lamella. Under large deformation, the Burgers Orientation Relationship (BOR,  $(0001)_\alpha // \{110\}_\beta$  and  $\langle 11-20 \rangle_\alpha // \langle 111 \rangle_\beta$ ) followed by alpha lamellae and beta matrix is destroyed, which can accelerate the formation of inter- $\alpha$  boundaries and the wedging of  $\beta$  phase into  $\alpha$  lamellae along intra- $\alpha$  boundaries, further separate  $\alpha$  lamellae [5,6]. In addition, a post-dynamic transformation of  $\alpha$  to  $\beta$  phase was also found during interrupted holding in two phase region driven by stored energy and stress [7,8].

According to the above mentioned phenomenon, the distribution of parent  $\beta$  grain is important to the orientations and sizes of the inherent  $\alpha$  colonies, but the microstructure of these parent  $\beta$  grains cannot be easily characterized directly at room temperature. The Electron Back-Scattered Diffraction (EBSD) technique in a Scanning Electron Microscope has been used to study  $\beta - \alpha$  phase transformation by in situ experiment [4,9] and parent  $\beta$  phase reconstruction from inherent  $\alpha$  orientations [10,11]. The post-processing reconstruction was developed by Humbert et al. [10,11]. The strategy to determine the parent  $\beta$  orientation is based on a misorientation criterion between neighboring  $\alpha$  variants. In fact, only a limited number of misorientations exist between  $\alpha$  variants inherited from the same  $\beta$  parent [12]. Triple junctions of  $\alpha$  grains that have misorientations compatible with a common parent orientations are identified first and used to compute the parent orientation. This model has been widely used to explore the texture of high-temperature parent  $\beta$  phase [13], variant selection of inherent  $\alpha$  phase [14] and macrozone formed by processing [15]. However, after subtransus deformation, due to that the formation of subgrain and orientation deviation inside  $\alpha$  grains breaks the misorientation criterion, traditional reconstruction method is invalid. To obtain the parent  $\beta$  grains of globularized sample, a denoising method is proposed in this work, which can directly reconstruct the  $\beta$  grains based on the restrained  $\beta$  phase not  $\alpha$  grains. The orientation of the reconstructed  $\beta$  grains can be further used to analyze the heterogeneous globularization mechanism of  $\alpha$  colonies.

In the present work, two samples with and without globularization processing were prepared for the parent  $\beta$  reconstruction. The new method to reconstruct  $\beta$  grain was performed by filling the restrained  $\beta$  phase with a EBSD denoising technique in MTEX toolbox [16], which was verified by comparing with the traditional reconstruction methods. Finally, the globularized microstructure was analyzed and the globularization mechanism was discussed with the help of the reconstructed  $\beta$  grain orientation.

## 2. Methodology

### 2.1. Materials

In the current work, the material used was Ti-6Al-4V alloy with a  $\beta$ -transus temperature of 995 °C. Two samples (Sample A and Sample B) were prepared to explore the grain reconstruction, of which the initial microstructures were shown in Fig. 1. Sample A, comprised of globular  $\alpha$  with the size of approximately 20  $\mu\text{m}$ , was obtained by the forging in  $\alpha - \beta$  phase region. Sample B was achieved by heat treatment above  $\beta$  transus followed by air cooling, which consists of colonies of lamellar- $\alpha$  (around 4  $\mu\text{m}$ ) inherited from millimetric equiaxed prior  $\beta$  grains.

To obtain different microstructures with  $\alpha$  lamellas inside small parent  $\beta$  grains and globularized  $\alpha$  grains inside larger parent  $\beta$  grains, following experimental processes were performed on the two samples. Sample A was annealed at 850 °C for 2 h followed by air cooling, while Sample B was performed under multiaxial hot cross-forging process by the Gleeble 3800 with MaxStrain II device. The preparation details of Sample B and MaxStrain test can be found in the previous work of Saint Jalme et al. [2]. The thermomechanical routine is presented in Fig. 2. The compression was carried out at the set temperature of 800 °C and the strain rate of 0.1  $\text{s}^{-1}$ . After a pre-deformation of 20%, two repeated compressions (first and second compressions) were interrupted at reduction ratios of 40% together with 90° rotation of the sample. The first and second compression axes are denoted respectively FCA and SCA. The specimen was cut along the central axis with the metallographic observation surface parallel to SCA.

Before EBSD characterization, the sample was mechanical ground until MASTERMET 2 colloidal silica, followed by electrolytic polishing using a solution of 5% perchloric acid, 35% butan-1-ol and 60% of methanol at 35V for 20 s at temperatures lower than 5 °C. The characterization was performed using Zeiss Supra-40 (Sample A) and JSM-F100 (Sample B) scanning electron microscope equipped with an EBSD camera with an accelerating voltage of 20 kV, a working distance of 15 mm and a step size of 0.2  $\mu\text{m}$ .

### 2.2. Reconstruction methods

MTEX and add-on software suite ORTools [17] were used to reconstruct the  $\beta$  grain based on inherited  $\alpha$  lamellas by traditional method [10,11]. The parent  $\beta$  grain of globularized  $\alpha$  microstructure was also reconstructed by filling the remnant  $\beta$  phase with denoising method. Smoothing spline method in MTEX toolbox is a denoising technique adapted from mathematical image analysis to the setting of orientation data [16], which consists of approximating noisy data  $O(x)$  by orientations  $\hat{O}(x)$  that minimize an energy functional

$$J(\hat{O}) = \sum_x \delta [\tilde{O}(x), \hat{O}(x)]^2 + \alpha \Delta \hat{O}(x)^2 \quad (1)$$

It is appropriate to separately apply the approximation for each grain and choose as the reference orientation the mean orientation of the grain.

The traditional reconstruction method based on  $\alpha$  lamellas has been widely used in the past few decades. It is usually very effective, because the  $\alpha$  phase can be well identified under EBSD. However, it still have some limitations: at least three types of  $\alpha$  variants with typical misorientation between them. Thus, the globularized or deformed  $\alpha$  microstructure is normally difficult to reconstructed. The new reconstruction method with denoising technique can be taken as a supplement to traditional method. Only mean orientations of reconstructed  $\beta$  grains can be obtained. In

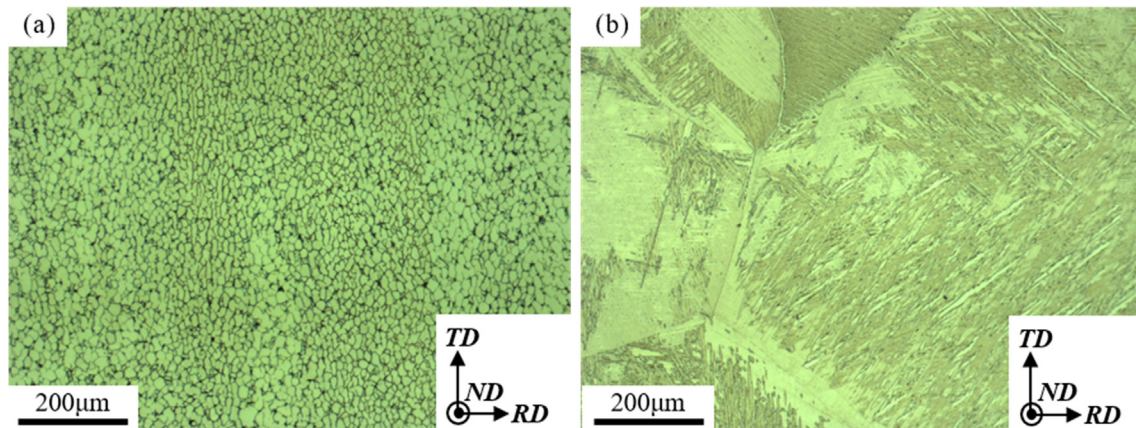


Fig. 1. Initial microstructures of (a) Sample A and (b) Sample B.

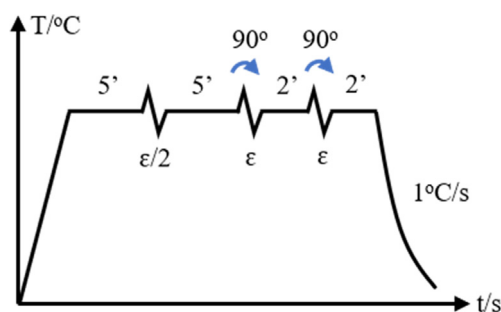


Fig. 2. Thermomechanical cycle on MaxStrain device ( $\varepsilon = 40\%$ ,  $\dot{\varepsilon} = 0.1 \text{ s}^{-1}$ ).

order to achieve this, enough remnant  $\beta$  phase need to be guaranteed in the EBSD measurement.

### 3. Results

#### 3.1. $\beta$ grain reconstruction of Sample A

The annealing process of Sample A initiates the globular  $\alpha$  into bimodal microstructure, globular primary  $\alpha$  grain ( $\alpha_p$ ) and secondary  $\alpha$  colonies ( $\alpha_s$ ), as shown in Fig. 3a. Normal direction (ND) axis was projected with the shown color bar. The corresponding inverse pole figure (IPF) map of  $\beta$  phase can be found in Fig. 3b. The residual  $\beta$  phase is located at  $\alpha$  boundaries and holds BOR in the lamella structure. The indexed phase fractions are respective 76.7% for  $\alpha$ , 0.8% for  $\beta$  phase and zero solutions of 22.5%.

The  $\beta$  grain reconstruction is performed based on the EBSD maps. First, the  $\beta$  grains are reconstructed by traditional method and shown in Fig. 3c with mean orientations. Most of the primary  $\alpha_p$  grains are not considered into the reconstruction process and defined by non-indexed particles. Fig. 3d presents the reconstruction map obtained by filling  $\beta$  phase in Fig. 3b with smoothing spline denoising method. Although Fig. 3d cannot separate the  $\alpha_p$  grains, it shows good match on both grain size and orientation between these two reconstruction methods. It can be concluded that, with smoothing spline method, the 0.8% restrained  $\beta$  phase in the EBSD map of Sample A is enough to reconstruct the parent grains. Moreover, the  $\beta$  phase reconstructed by misorientation criterion (Fig. 3c) can be regarded as high-temperature  $\beta$  phase, while by smoothing spline method (Fig. 3d) room temperature  $\beta$  phase is obtained. The matched results between them means that the orientation of high-temperature  $\beta$  phase can be maintained during cooling.

To further evaluate the correctness of denoising method, the orientations and grain sizes of 17 selected grains in Fig. 3c and d are calculated and compared in the histograms. Fig. 4a shows the distribution of disorientation angles between the grain orientations obtained by two reconstruction methods. As an example, for Grain 1, the Euler angles in Fig. 3c are  $(267.2^\circ, 101.7^\circ, 113.8^\circ)$  and  $(202.0^\circ, 26.5^\circ, 152.8^\circ)$  in Fig. 3d, which can be directly obtained from the reconstruction procedures. The disorientation angle between them is  $0.15^\circ$ . In general, all the disorientation values are lower than  $1^\circ$  within the allowable error range, although the distribution of disorientation angles in Fig. 4a shows some fluctuations. In addition, the grain sizes ( $\mu\text{m}^2$ ) in both reconstruction maps are compared in Fig. 4b. The size of each grain calculated by denoising reconstruction method is slightly larger than that by traditional method, because primary  $\alpha_p$  grain in Fig. 3c is excluded when calculating the grain area in traditional method. Although there is a certain gap between the grain area calculated by these two methods, the denoising method can still be considered accurate to determine the parent  $\beta$  grain orientation and microstructure.

#### 3.2. $\beta$ grain reconstruction of Sample B

The microstructure of Sample B after multi-axial compression test is presented by forward scatter detector (FSD) image in Fig. 5a. The observation surface is parallel to the second compression axis (SCA//Y and FCA//Z). In the figure, the grain boundary  $\alpha$  ( $\text{GB}\alpha$ ) formed along prior  $\beta$  boundary is marked by a red dotted line. It can be found in the FSD image that the deformation modes are different above and below the prior  $\beta$  boundary. Numerous distorted and thick  $\alpha$  lamellas appear at the upside of the  $\beta$  boundary to relax the stress concentration. However, below the boundary, many finer  $\text{GB}\alpha$ s can be found, which indicates that the recrystallization of the large prior  $\beta$  grain occurs during hot compression. The magnification image of a recrystallized  $\beta$  grain labeled in the yellow box (Fig. 5a) is presented in Fig. 5b, where the boundary is marked by a solid red line. Inherent  $\alpha$  lamellas can be also observed inside the  $\beta$  grain.

In fact, most of the  $\alpha$  lamellas have been broken up into globularized grains after the thermomechanical cycle, which are not clear under FSD map but can be better observed in Fig. 6a (corresponding IPF map of Fig. 5a). The  $\alpha$  and  $\beta$  phase fractions are around 91.4% and 2.0%, respectively. The  $\alpha$  globularization will be discussed in Section 4. The IPF map of residual  $\beta$  phase is shown in Fig. 6b. Below the prior  $\beta$  grain boundary (dotted black line), the recrystallized  $\beta$  boundaries (solid black lines) are drawn by the combination of  $\text{GB}\alpha$  in FSD image (Fig. 5a) and the orientation of

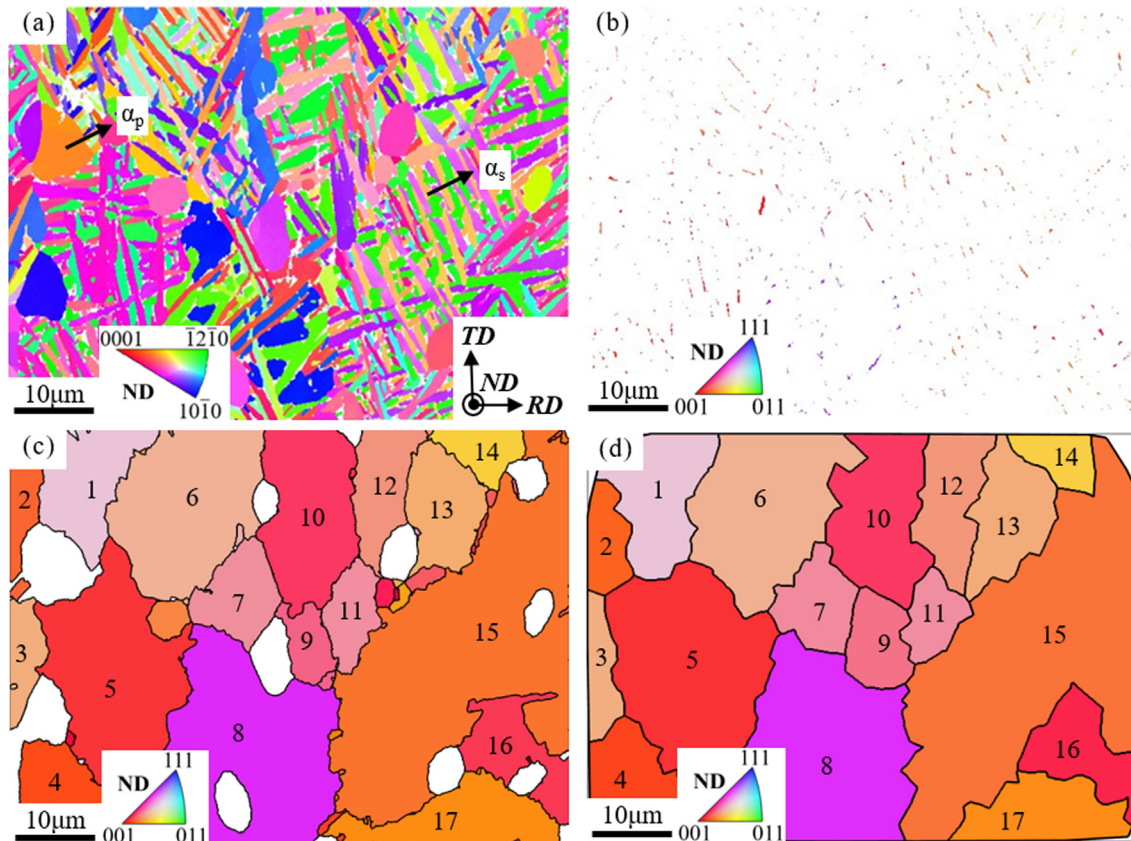


Fig. 3. IPF maps of Sample A. (a)  $\alpha$  phase and (b)  $\beta$  phase.  $\alpha_p$  is globular primary  $\alpha$  grain and  $\alpha_s$  represents secondary  $\alpha$  colony. (c) and (d) are IPF maps of parent  $\beta$  grains reconstructed by misorientation criterion and denoising method, respectively. The numbers of 17 grains in (c) and equivalent grains in (d) are labeled.

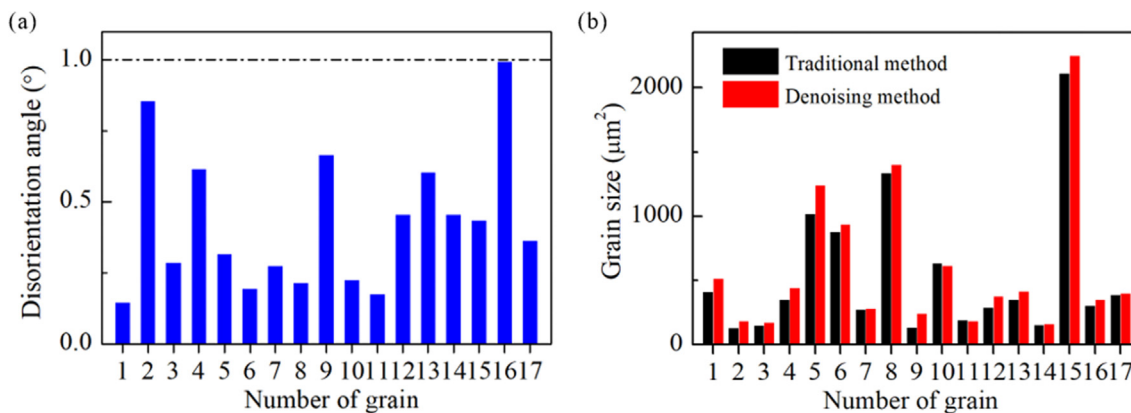
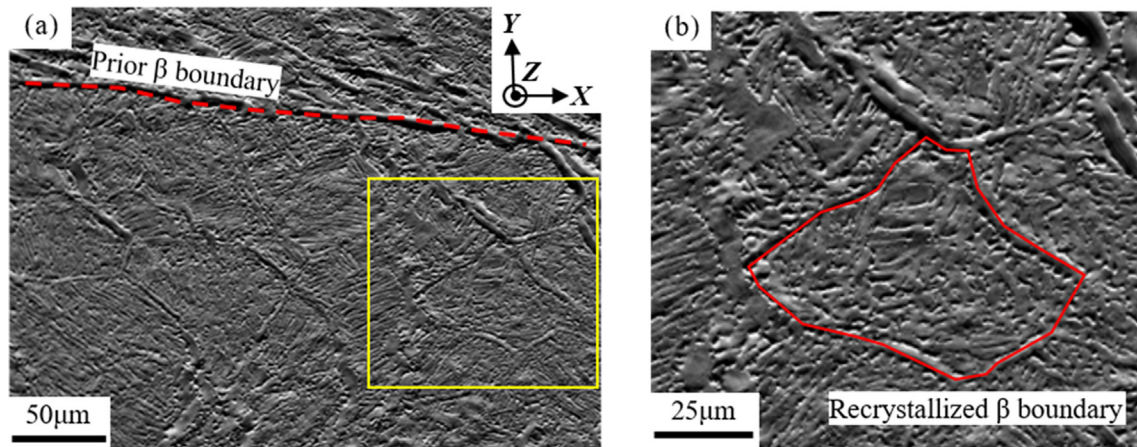


Fig. 4. Distributions of (a) disorientation angle and (b) grain size. The orientations and sizes of the 17 grain are calculated by traditional and denoising reconstruction method.

remained  $\beta$  phase in Fig. 6b. A total of 13 parent  $\beta$  grains are drawn. The magnification image of the area in the red box (Fig. 6b) is presented in Fig. 6c. It can be seen that, inside each recrystallized  $\beta$  grain, the orientations are close but there also appears local  $\beta$  recrystallization due to stress concentration. Based on the EBSD map of remnant  $\beta$  phase (Fig. 6b), parent  $\beta$  grains can be generally reconstructed by smoothing spline denoising method and colored by mean orientations, as shown in Fig. 6d. The local recrystallization inside each  $\beta$  grain is considered during the calculation of mean orientation. It can be found that the grain shapes of most of the reconstructed  $\beta$  grains can well match with that labeled by black lines in Fig. 6b. However, some  $\beta$  grains (Grain 3 and Grain 11) cannot be correctly reconstructed due to severe internal

recrystallization. Besides, above the prior  $\beta$  boundary, there is not  $\beta$  recrystallization observed in Fig. 5a, thus the reconstruction result does not make sense.

Due to the heterogeneous stress during deformation, the local orientation of  $\beta$  grain can deviate from the mean orientation calculated by denoising method. Thus, to verify the accuracy of the reconstruction results, the deviation between local and mean orientations of each grain should be calculated. To do this, the orientation-trace method of Zhao et al. [18] is used, which can determine the local  $\beta$  orientation from one  $\alpha$  variant orientation with interface trace direction. The interface boundary structure between transformed  $\alpha$  lath and parent  $\beta$  grain has been established previously [19]. The interface results from regularly spaced



**Fig. 5.** (a) FSD image of Sample B. (b) The higher-magnification FSD image of the area in the yellow box. (For interpretation of the references to color in this figure legend, the reader is referred to the web version of this article.)

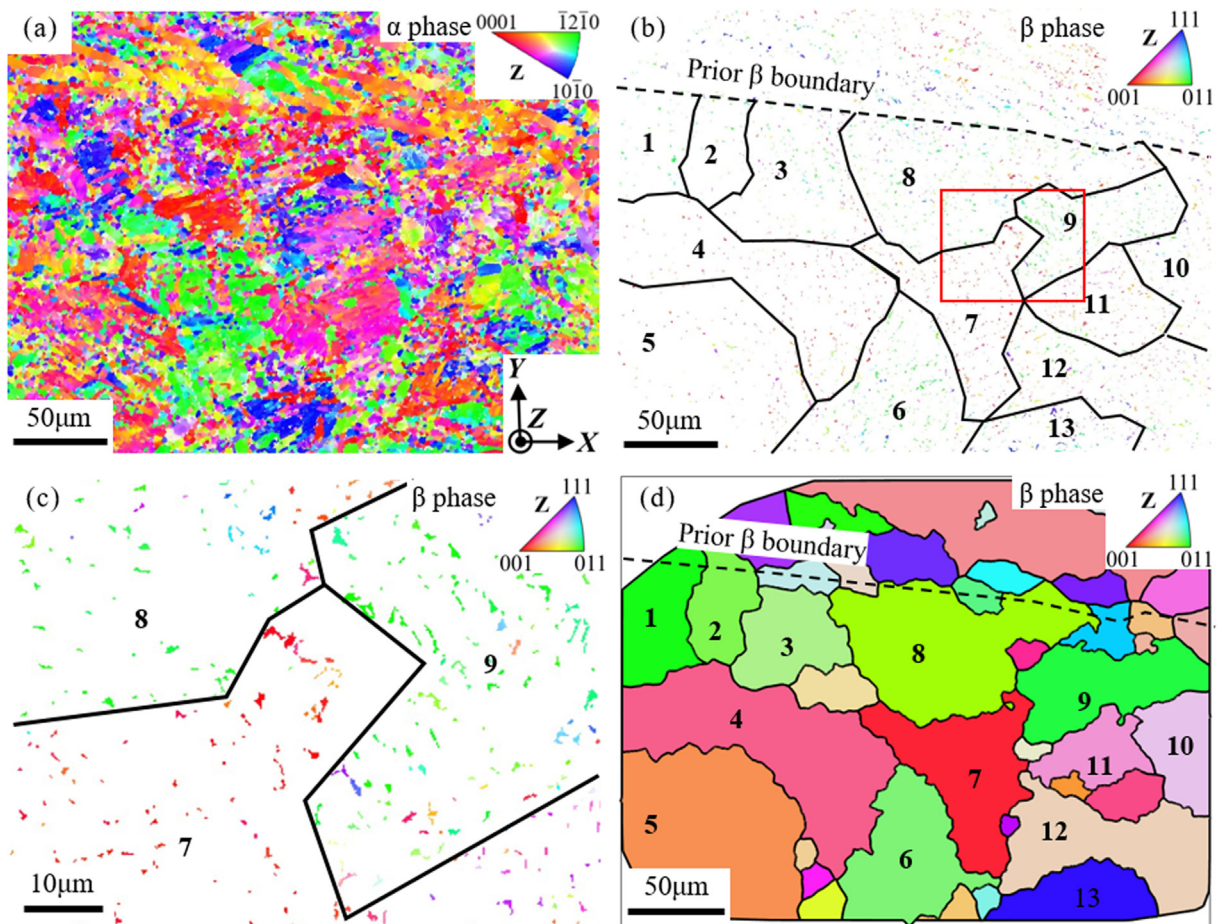


**Fig. 6.** IPF map of Sample B, (a)  $\alpha$  phase and (b)  $\beta$  phase. (c) The higher-magnification IPF map of the area in the red box of (b). (d) IPF map of parent  $\beta$  grains reconstructed from (b) by denoising method. The  $\beta$  grain boundaries are marked by black lines. The numbers of 13 grains in (b) and equivalent grains in (d) are labeled. (For interpretation of the references to color in this figure legend, the reader is referred to the web version of this article.)

atomic steps with  $[1100]_{\alpha} // [11\bar{2}]_{\beta}$  terraces. In near  $\alpha$ -titanium alloys, the broad face of the  $\alpha$ -plate has an irrational habit plane close to  $(11\bar{15}40)_{\alpha} // (11\bar{11}13)_{\beta}$ . The  $\beta$  orientation of Grain 8 is calculated with this method as an example and then compared with the reconstruction result in Fig. 6d. Fig. 7a shows the EBSD

map (IPF map plus band contrast) of Grain 8. The globularized grains make it difficult to determine the orientations of  $\alpha$  colonies. So the  $\alpha$  grains are detected by the critical misorientation of  $15^{\circ}$  and colored by mean orientation. According to the research of Fan et al. [6], the grain boundaries with  $2^{\circ}$ - $15^{\circ}$  are subgrain/low angle boundaries (LAGBs) and those of  $> 15^{\circ}$  are high angle grain boundaries (HAGBs). After that, the mean orientation of  $\alpha$  variant

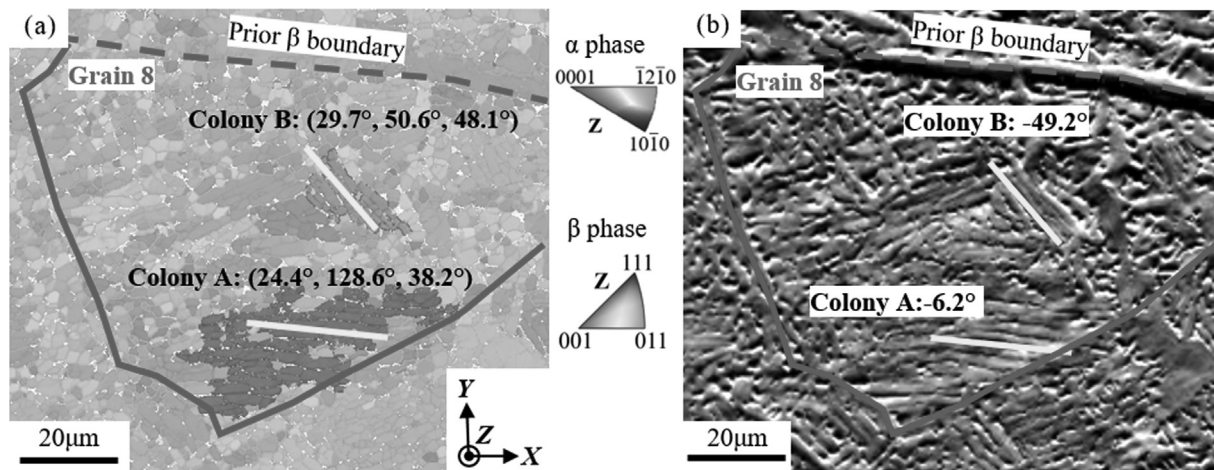


**Fig. 7.** (a) EBSD band contrast image overlaid with an IPF map colored by the shown color bars. (b) FSD image. The boundary of Grain 8 is labeled by red line. (For interpretation of the references to color in this figure legend, the reader is referred to the web version of this article.)

can be obtained. The lamella trace is not clear in EBSD map due to the globularization process, but can be better determined under FSD image. Two  $\alpha$  colonies with clear traces in Fig. 7b are chosen with the mean orientations of Colony A ( $24.4^\circ$ ,  $128.6^\circ$ ,  $38.2^\circ$ ) and Colony B ( $29.7^\circ$ ,  $50.6^\circ$ ,  $48.1^\circ$ ). The interface traces of  $\alpha$  lamellas in Colony A and Colony B are labeled by solid yellow lines, which are respective  $-6.2^\circ$  and  $-49.2^\circ$  from horizontal direction (X axis).

Using the method of [18], six potential parent  $\beta$  orientations of Colony A and Colony B are calculated and shown in Table 1. The interface plane normals of the  $\alpha$  variants corresponding to the six  $\beta$  variants are expressed in terms of the sample coordinates ( $Y//SCA$  and  $Z//FCA$ ). Then, the  $(11\ 11\ 13)_\beta$  interface trace angles can be obtained. Comparing the calculated trace directions with the measured ones ( $-6.2^\circ$  and  $-49.2^\circ$ ), the trace angle of respective  $V_{4\beta}$  ( $-9.9^\circ$ ) and  $V_{6\beta}$  ( $-58.4^\circ$ ) are the closest. Thus, the local  $\beta$  orientations of Colony A and Colony B can be obtained with the Euler angles of ( $243.7^\circ$ ,  $134.1^\circ$ ,  $74.7^\circ$ ) and ( $265.3^\circ$ ,  $55.5^\circ$ ,  $185.4^\circ$ ). The disorientation angles between the two local  $\beta$  orientations and mean orientation of Grain 8 ( $254.4^\circ$ ,  $54.8^\circ$ ,  $90.3^\circ$ ) are  $14.8^\circ$  and  $14.4^\circ$ , which are larger than the disorientation angles for Sample A in Fig. 4a (lower than  $1^\circ$ ). It is reasonable for Sample B subjected to large deformation. Due to the accumulated misorientations and substructures inside  $\alpha$  lamellas of Sample B, the orientation of  $\alpha$  colony used to calculate parent  $\beta$  grain is the mean orientation of  $\alpha$  grains with the  $15^\circ$  critical misorientation. Besides, the local recrystallization of  $\beta$  grain can also lead to the deviation of mean orientation during  $\beta$  reconstruction.

As for the other  $\beta$  grains, the selected  $\alpha$  colonies (1 or 2 colonies for each grain) and corresponding interface traces are shown in Fig. 8a and Fig. 8b, respectively. Grain 3 and Grain 11 are excluded due to non unique reconstructed orientations inside the grains (Fig. 6d). The orientations and trace angles of each colony can be

found in Table 2. Based on the orientations and the trace directions, the local orientations of all the  $\beta$  grains can be obtained. Then, the reconstructed  $\beta$  grain orientations in Fig. 6d are compared with the calculated results by the values of disorientation angles. The distribution of disorientation angle is shown in Fig. 9. It can be seen that all the disorientation angles between mean and local orientations are lower than  $20^\circ$ . The minimum and maximum disorientation angles are respective  $6.0^\circ$  and  $17.3^\circ$  for Grain 10 and Grain 12. The large orientation deviation below  $20^\circ$  inside parent  $\beta$  grains is acceptable because of the accumulated dislocation inside both  $\alpha$  and  $\beta$  phase during hot deformation process in the two-phase region. Therefore, the  $\beta$  grain reconstruction by smoothing spline method is feasible for  $\alpha$  globularized sample.

#### 4. Discussion

The globularized microstructure produced by hot deformation in the  $\alpha + \beta$  two phases region can lead to a better balance between strength and ductility as well as a high fatigue strength. The globularization level during thermomechanical treatment significant depends on process parameters, such as strain rate, temperature and holding time. Kim et al. [20] proposed that the strain rate of  $0.1\ s^{-1}$  results in the highest level of flow softening behaviors, which corresponds to globularization. The deformation below  $900^\circ C$  generally leads to better globularization by dynamic recrystallization mechanism [21]. Besides, all of the interrupted strain, holding time and loading pass can increase the globularization efficiency [6].

In this work, Sample B is deformed under the strain rate of  $0.1\ s^{-1}$  at  $800^\circ C$  (around  $850^\circ C$  at the sample center measured by thermocouple). During deformation, both grain boundary distribution and grain aspect ratio can be changed. The  $\alpha$ - $\alpha$  boundary misorientation angle distribution of the initial and deformed Sam-

**Table 1**  
Possible  $\beta$  orientations and corresponding interface directions of Colony A and Colony B.

$\beta$ variant	Colony A ( $24.4^\circ$ , $128.6^\circ$ , $38.2^\circ$ )		Colony B ( $29.7^\circ$ , $50.6^\circ$ , $48.1^\circ$ )	
	$\beta$ grain orientation	$\alpha$ trace angle	$\beta$ grain orientation	$\alpha$ trace angle
$V_{1\beta}$	( $327.8^\circ$ , $55.4^\circ$ , $265.8^\circ$ )	$35.0^\circ$	( $274.4^\circ$ , $62.5^\circ$ , $0.7^\circ$ )	$34.8^\circ$
$V_{2\beta}$	<b>(<math>243.7^\circ</math>, <math>134.1^\circ</math>, <math>74.7^\circ</math>)</b>	<b><math>-9.9^\circ</math></b>	( $3.8^\circ$ , $137.6^\circ$ , $205.2^\circ$ )	$75.3^\circ$
$V_{3\beta}$	( $285.9^\circ$ , $100.5^\circ$ , $275.6^\circ$ )	$-40.7^\circ$	( $315.0^\circ$ , $107.8^\circ$ , $356.8^\circ$ )	$-78.0^\circ$
$V_{4\beta}$	( $292.6^\circ$ , $92.3^\circ$ , $96.4^\circ$ )	$74.7^\circ$	( $307.9^\circ$ , $99.9^\circ$ , $175.1^\circ$ )	$-9.1^\circ$
$V_{5\beta}$	( $229.8^\circ$ , $138.5^\circ$ , $244.6^\circ$ )	$-80.7^\circ$	( $19.3^\circ$ , $140.1^\circ$ , $37.0^\circ$ )	$-37.7^\circ$
$V_{6\beta}$	( $338.3^\circ$ , $49.0^\circ$ , $79.3^\circ$ )	$-61.3^\circ$	<b>(<math>265.3^\circ</math>, <math>55.5^\circ</math>, <math>185.4^\circ</math>)</b>	<b><math>-58.4^\circ</math></b>

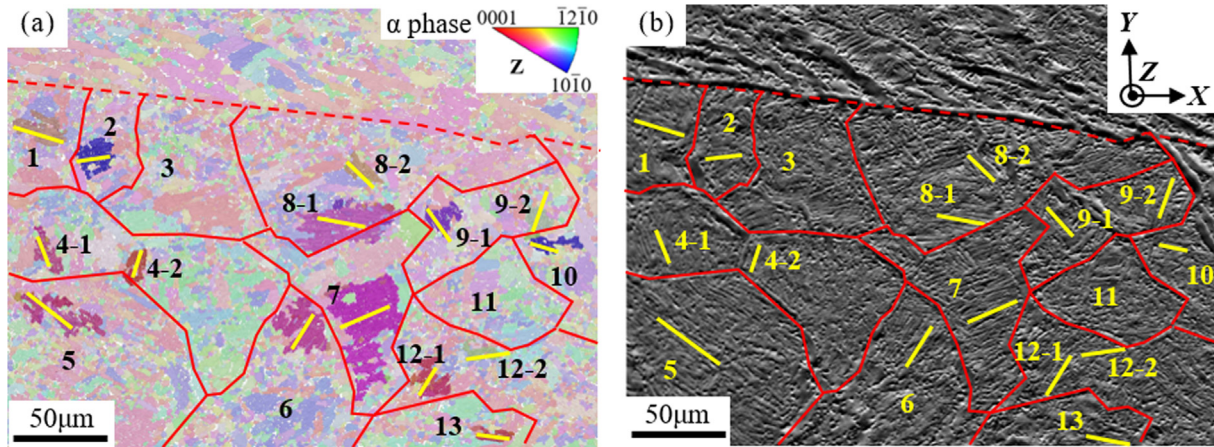


**Fig. 8.** (a) EBSD band contrast image overlaid with an IPF map colored by the shown color bars. (b) FSD image. The parent  $\beta$  grains are labeled by the white or red lines. The interface traces of selected colonies are marked by yellow lines. (For interpretation of the references to color in this figure legend, the reader is referred to the web version of this article.)

**Table 2**

The details of the orientations and trace angles used to verify the reconstruction results.

Grain number	Mean $\beta$ orientation	Actual $\alpha$ trace angle	Selected $\alpha$ colony orientation	Local $\beta$ orientation	Calculated $\alpha$ trace angle
1	37.4°, 44.1°, 91.2°	-17.3°	154.4°, 127.5°, 14.3°	38.1°, 120.0°, 90.3°	-24.2°
2	77.3°, 38.3°, 4.7°	6.1°	81.3°, 81.0°, 28.1°	350.2°, 83.0°, 144.1°	-0.4°
4-1	351.8°, 14.5°, 57.6°	-69.4°	139.9°, 30.9°, 42.2°	55.9°, 93.6°, 194.3°	-77.2°
4-2		72.0°	53.0°, 153.4°, 45.2°	314.1°, 94.4°, 71.3°	85.8°
5	102.7°, 13.5°, 76.5°	-38.8°	18.0°, 47.1°, 22.1°	279.0°, 80.4°, 178.7°	-44.9°
6	317.6°, 38.9°, 352.6°	59.9°	70.2°, 134.2°, 31.9°	293.6°, 126.8°, 74.5°	46.8°
7	46.3°, 5.3°, 122.9°	23.0°	72.6°, 45.0°, 30.1°	338.9°, 86.4°, 180.1°	17.8°
8-1	254.4°, 54.8°, 90.3°	-10.2°	24.4°, 128.6°, 38.2°	243.7°, 134.1°, 74.7°	-9.9°
8-2		-49.2°	29.7°, 50.6°, 48.1°	265.3°, 55.5°, 185.4°	-58.4°
9-1	218.9°, 46.5°, 356.3°	-55.4°	90.6°, 63.7°, 28.9°	31.6°, 136.2°, 174.8°	-60.5°
9-2		69.9°	162.5°, 116.4°, 13.4°	45.7°, 132.3°, 278.1°	73.1°
10	218.7°, 31.2°, 30.0°	-15.3°	112.5°, 81.6°, 30.4°	34.3°, 144.3°, 149.5°	-5.7°
12-1	71.1°, 24.2°, 20.7°	58.2°	109.0°, 150.3°, 31.5°	12.4°, 94.3°, 252.4°	58.0°
12-2		8.3°	138.0°, 116.8°, 14.0°	100.2°, 32.6°, 258.2°	11.0°
13	357.0°, 50.7°, 45.5°	-8.8°	91.9°, 150.5°, 27.4°	302.6°, 115.9°, 239.6°	-9.1°

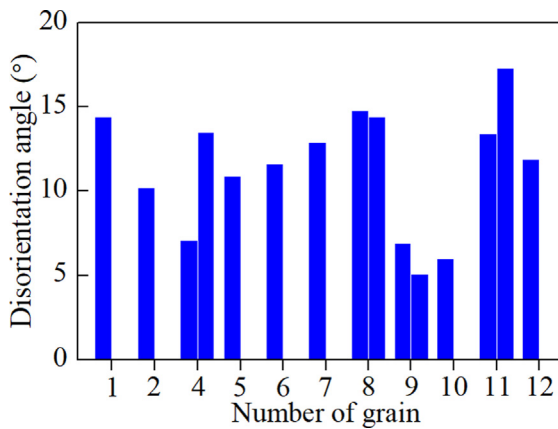


**Fig. 9.** Statistics of disorientation angle between the reconstruction and calculated results.

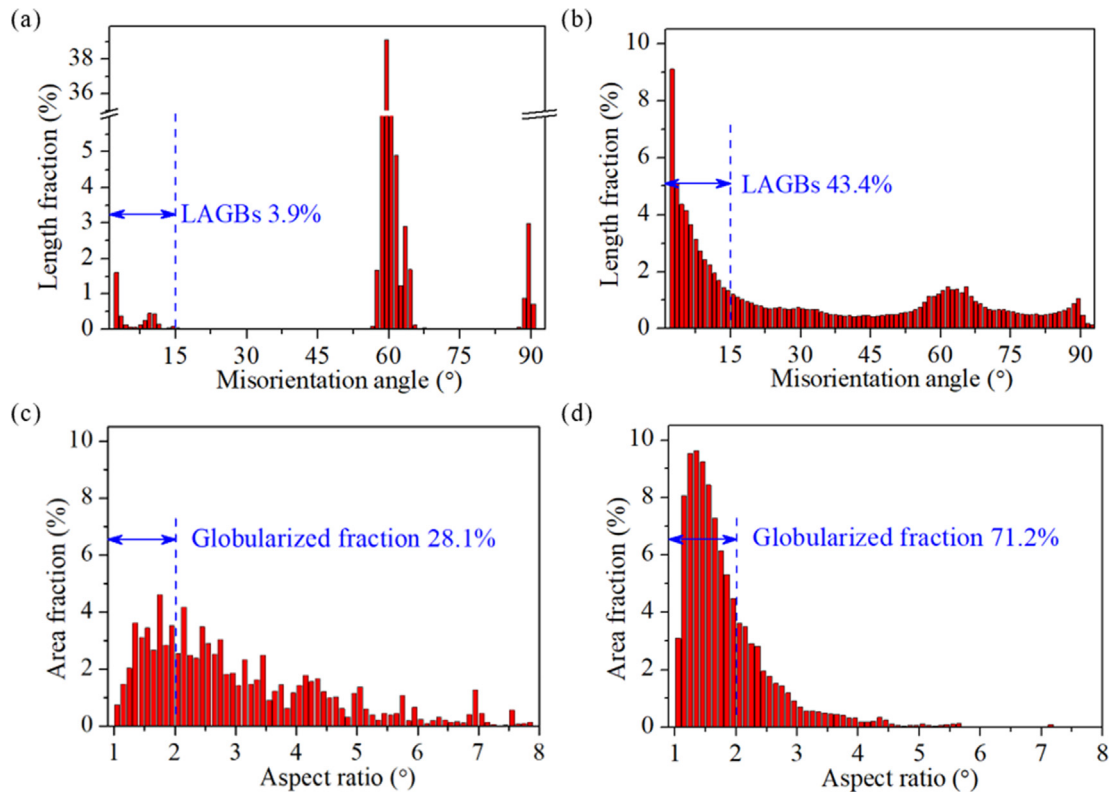
ple B are compared in Fig. 10a and b, respectively. As shown in Fig. 10a, three sharp and intense peaks appear at misorientation angles of  $\sim 10^\circ$ ,  $55\text{--}65^\circ$  and  $\sim 90^\circ$ . Haghdadi et al. [22] studied grain boundary plane characteristics of the  $\alpha$ - $\alpha$  intervariant interfaces. The peaks correspond to different intervariant boundaries, produced by the self-accommodation during the  $\beta$  to  $\alpha$  phase transformation. After hot compression, the peaks become so weak in

Fig. 10b, which indicates that the accumulated stress in the deformed sample can influence the accommodation behavior during phase transformation and deviate the intervariant boundaries angles. The discrete misorientation distribution finally leads to the failure of traditional reconstruction method. Besides, the LAGBs fraction of deformed Sample B (43.4%) is much higher than the initial sample (3.9%). Therefore, the accumulated crystal defects and the formation of subgrains during compression increase the fraction of LAGBs.

It can be found directly from Fig. 6a, that obvious  $\alpha$  globularization process has been obtained after multi-axial compression test. Fig. 10c and d show the area fraction as a function of the grain shape aspect ratios of the initial and deformed samples. The grain shape aspect ratio ( $\lambda$ ) is defined as the length of the major axis ( $a$ ) divided by the length of the minor axis ( $b$ ) of the ellipse fitting to a certain grain.

$$\lambda = a/b \quad (2)$$

The  $\alpha$  grains with aspect ratio less than 2 are taken as a sign of globularization. Indeed, the globularization fraction significantly increases from 28.1% before deformation to 71.2% after hot compression. Fan et al. [6] explored the acceleration of globularization during interrupted compression. The globularization fraction increases to 77.9% after sextuple-hit deformation with the accumulated reduction ratio of 60%. In this work, the multi-axial compression can also effectively improve the globularization similar to



**Fig. 10.** Distributions of (a)  $\alpha$ - $\alpha$  boundary misorientation angle of initial Sample B, (b)  $\alpha$ - $\alpha$  boundary misorientation angle of deformed Sample B, (c) grain shape aspect ratio of initial Sample B and (d) grain shape aspect ratio of deformed Sample B.

the increase of the number of deformation pass. In fact, the globularization efficiency is not only related to the relative crystallographic orientation but the geometrical orientation of the alpha colony as well [23]. The geometrical orientation ( $\theta$ ) was calculated by the angle between long axis of  $\alpha$  lath on the observation surface and compression axis. The deviated angle of  $c$ -axis from compression axis ( $\varphi$ ) represents crystal orientation. The inclined colonies with respect to the loading direction together with special crystal orientation are more favorable for both prism and basal slip systems and thus can improve the globularization efficiency. Under multi-axial compression, more slip systems can be activated inside  $\alpha$  colonies, leading to the higher globularization fraction. In addition,

according to Fig. 6b, significant  $\beta$  recrystallization happens inside the large prior  $\beta$  grain, which can be facilitated by multi-axial deformation. In fact, the BOR can be maintained during deformation due to the fact that the  $\alpha_p/\beta$  interface can accommodate some slip systems of  $\alpha_p$  and adjacent  $\beta$  grain [15]. Thus, the deformation-induced rotation of the  $\alpha_p$  and  $\beta$  grain can be synchronized. The weakened  $\beta$  texture due to the recrystallization can further improve the  $\alpha$  globularization homogeneity and restrain the formation of macrozone.

Although the globularization fraction is higher after multi-axial compression, heterogeneity from colony to colony still exists. The soft colonies undergo larger deformation and they get better glob-

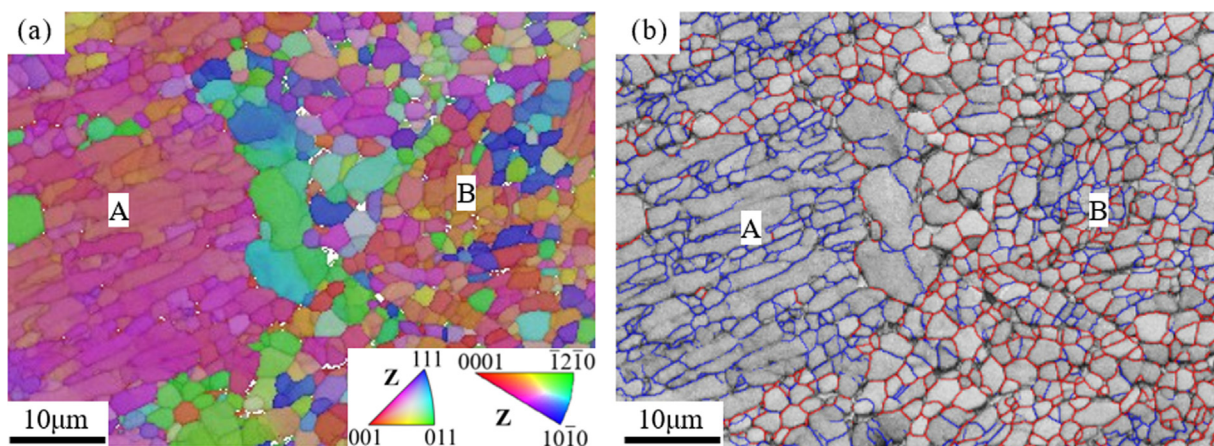


**Fig. 11.** EBSD maps of the heterogeneous area of Sample B, (a) Band contrast image overlaid with an IPF map colored by the shown color bars. (b) Band contrast map with colored grain boundaries. The red and blue lines represent HAGBs and LAGBs, respectively. (For interpretation of the references to color in this figure legend, the reader is referred to the web version of this article.)

ularized than the hard ones [24]. An example of heterogeneous globularization will be briefly discussed with the help of the reconstructed  $\beta$  orientation by denoising technique.

An area with heterogeneous microstructure near the boundary between Grain 7 and Grain 9 (Fig. 6) is shown in Fig. 11. Fig. 11a is the band contrast image overlaid with IPF map. The Colony A is globularized with similar orientations, while globularized Colony B has large orientation spread. Both geometrical and crystallographic orientations [23,24] should be considered as the reason for the less globularized fraction of Colony A. The mean orientation of parent  $\beta$  grain (Grain 7) for Colony A is  $(46.3^\circ, 5.3^\circ, 122.9^\circ)$  as shown in Table 2. Then, by combining the local orientation and the trace direction of Colony A, the direction of  $(11 \bar{1} 13)_\beta$  interface of  $\alpha$  variant can be quickly determined. The interface plane normal of  $\alpha$  variant in Colony A is  $(4.2, -6.3, -6.5)$  under the sample coordinates ( $Y//SCA$  and  $Z//FCA$ ). The trace direction of the interface plane on  $X$ - $Y$  and  $X$ - $Z$  surfaces are  $(6.3, 4.2)$  and  $(6.5, 4.2)$ . Then, the geometrical angles ( $\theta$ ) between trace direction and  $SCA/FCA$  can be obtained. The angles ( $\varphi$ ) are between the  $c$ -axis of Colony A and compression axes. Therefore, the  $(\theta, \varphi)$  of Colony A with respected to  $SCA$  and  $FCA$  are respective  $(56.3^\circ, 79.9^\circ)$  and  $(57.1^\circ, 49.5^\circ)$ . In addition,  $50^\circ < \theta < 60^\circ$  and  $15^\circ < \varphi < 75^\circ$  are the favorable conditions for globularization [23,24]. The angle  $\varphi$  of Colony A with respected to  $SCA$  is  $79.9^\circ > 75^\circ$ . Therefore, during the second compression, the  $\alpha$  lath in Colony A is unfavorable for strain partitioning, and it is also difficult to activate both prism and basal slip systems for efficient breakdown.

Fig. 11b shows the band contrast map with colored grain boundaries. The red lines represent the HAGBs ( $>15^\circ$ ), while the blue lines are LAGBs ( $2^\circ$ – $15^\circ$ ). Due to the lower globularization efficiency, the microstructure of Colony A can be regarded as the beginning of globularization process. During deformation, the accumulated crystal defects in  $\alpha/\beta$  can finally lead to the collapse of stable BOR, which results in the LAGBs (more inter-lamellar boundary than intra lamellar boundary). With the continuous dislocation absorption, the intra-lamellar boundary increases. Finally, significant reticulate substructure can be observed with most of HAGBs like Colony B.

## 5. Conclusions

This work proposes a new idea to reconstruct  $\beta$  grain of titanium alloy with the restrained  $\beta$  phase by the method of MTEX smoothing splines. Two samples with  $\alpha$  lamella and globularized microstructures are presented and discussed. The reconstruction results are compared with the orientation calculated by the usual reconstruction methods. The following conclusions can be drawn from this work:

- (1) The mean orientations of parent  $\beta$  grains of the sample with bimodal microstructure are reconstructed by both the traditional misorientation criterion and smoothing spline methods. By comparing the microstructures obtained by these two methods, both the grain sizes and orientations correspond well. Thus, the smoothing spline method also shows a good ability to reconstruct the parent  $\beta$  phase of bimodal or lamella-shaped sample as traditional reconstruction method.
- (2) The second sample with globularized  $\alpha$  grains is deformed by multi-axial hot compression. Obvious  $\beta$  recrystallization also happens inside the large prior  $\beta$  grain during deformation. The mean orientation of recrystallized  $\beta$  grain is well reconstructed by smoothing spline, and it is further validated by the calculation of local  $\beta$  grain orientation with orientation-trace method. There appears maximum  $20^\circ$

misorientation inside parent  $\beta$  grains due to the accumulated orientation deviation inside both remnant  $\beta$  and  $\alpha$  grains during hot deformation.

- (3) The multi-axial hot compression test can effectively achieve high globularized fraction around 71.2%. Although there also appears local heterogeneity between different  $\alpha$  colonies, the change of deformation direction and the appearance of  $\beta$  recrystallization can well suppressed the formation of macrozone and facilitate homogeneous globularization process.

## Declaration of Competing Interest

The authors declare that they have no known competing financial interests or personal relationships that could have appeared to influence the work reported in this paper.

## Acknowledgements

The authors acknowledge the financial support from agence nationale de la recherche ANR of France (Grant no. ANR-18-CE08-0027). The industrial partner, Aubert & Duval, is gratefully acknowledged for the contributions to this research.

## References

- [1] D. Banerjee, J.C. Williams, Perspectives on titanium science and technology, *Acta Mater.* 61 (3) (2013) 844–879.
- [2] M.S. Jalme, C. Desrayaud, J. Favre, D. Fabrègue, S. Dancette, C. Schuman, J.S. Lecomte, E. Archaud, C. Dumont, Microstructure Evolution during Multiaxial Processing of TAGV, *Mater. Sci. Forum, Trans Tech Publ* 1016 (2021) 1211–1217.
- [3] S.L. Semiatin, F. Montheillet, G. Shen, J.J. Jonas, Self-consistent modeling of the flow behavior of wrought alpha/beta titanium alloys under isothermal and nonisothermal hot-working conditions, *Metall. Mater. Trans. A, Phys. Metall. Mater. Sci.* 33 (8) (2002) 2719–2727.
- [4] E. Alabort, P. Kontis, D. Barba, K. Dragnevski, R.C. Reed, On the mechanisms of superplasticity in Ti–6Al–4V, *Acta Mater.* 105 (2016) 449–463.
- [5] L. Wang, X.G. Fan, M. Zhan, X.Q. Jiang, Y.F. Liang, H.J. Zheng, W.J. Liang, Revisiting the lamellar globularization behavior of a two-phase titanium alloy from the perspective of deformation modes, *J. Mater. Process. Technol.* 289 (2021) 116963.
- [6] X.G. Fan, H.J. Zheng, Y. Zhang, Z.Q. Zhang, P.F. Gao, M. Zhan, J. Liu, Acceleration of globularization during interrupted compression of a two-phase titanium alloy, *Mater. Sci. Eng. A.* 720 (2018) 214–224.
- [7] X. Ji, B. Guo, F. Jiang, H. Yu, D. Fu, J. Teng, H. Zhang, J.J. Jonas, Accelerated flow softening and dynamic transformation of Ti–6Al–4V alloy in two-phase region during hot deformation via coarsening  $\alpha$  grain, *J. Mater. Sci. Technol.* 36 (2020) 160–166.
- [8] X. Ji, H. Yu, B. Guo, F. Jiang, D. Fu, J. Teng, H. Zhang, J.J. Jonas, Post-dynamic  $\alpha$  to  $\beta$  phase transformation and reverse transformation of Ti–5Al–3V alloy after hot deformation in two phase region, *Mater. Des.* 188 (2020) 108466.
- [9] G.G.E. Seward, S. Celotto, D.J. Prior, J. Wheeler, R.C. Pond, In situ SEM-EBSD observations of the hcp to bcc phase transformation in commercially pure titanium, *Acta Mater.* 52 (4) (2004) 821–832.
- [10] M. Humbert, F. Wagner, H. Moustahfid, C. Esling, Determination of the orientation of a parent  $\beta$  grain from the orientations of the inherited  $\alpha$  plates in the phase transformation from body-centred cubic to hexagonal close packed, *J. Appl. Crystallogr.* 28 (5) (1995) 571–576.
- [11] M. Humbert, N. Gey, The calculation of a parent grain orientation from inherited variants for approximate (bcc–hcp) orientation relations, *J. Appl. Crystallogr.* 35 (4) (2002) 401–405.
- [12] L. Germain, N. Gey, M. Humbert, Reliability of reconstructed  $\beta$ -orientation maps in titanium alloys, *Ultramicroscopy* 107 (12) (2007) 1129–1135.
- [13] Z.B. Zhao, Q.J. Wang, Q.M. Hu, J.R. Liu, B.B. Yu, R. Yang, Effect of  $\beta$  (110) texture intensity on  $\alpha$ -variant selection and microstructure morphology during  $\beta \rightarrow \alpha$  phase transformation in near  $\alpha$  titanium alloy, *Acta Mater.* 126 (2017) 372–382.
- [14] N. Stanford, P.S. Bate, Crystallographic variant selection in Ti–6Al–4V, *Acta Mater.* 52 (17) (2004) 5215–5224.
- [15] L. Germain, N. Gey, M. Humbert, P. Vo, M. Jahazi, P. Bocher, Texture heterogeneities induced by subtransus processing of near  $\alpha$  titanium alloys, *Acta Mater.* 56 (16) (2008) 4298–4308.
- [16] R. Hielscher, C.B. Silbermann, E. Schmidl, J. Ihlemann, Denoising of crystal orientation maps, *J. Appl. Crystallogr.* 52 (5) (2019) 984–996.

- [17] F. Niessen, T. Nyssönen, A.A. Gazder, R. Hielscher, Parent grain reconstruction from partially or fully transformed microstructures in MTEX, ArXiv Prepr. ArXiv2104.14603. (2021).
- [18] Z.B. Zhao, Q.J. Wang, H. Wang, J.R. Liu, R. Yang, Determining the orientation of parent  $\beta$  grain from one  $\alpha$  variant in titanium alloys, *J. Appl. Crystallogr.* 51 (4) (2018) 1125–1132.
- [19] S. Zherebtsov, G. Salishchev, S. Lee Semiatin, Loss of coherency of the alpha/beta interface boundary in titanium alloys during deformation, *Philos. Mag. Lett.* 90 (12) (2010) 903–914.
- [20] J.H. Kim, S.L. Semiatin, C.S. Lee, Constitutive analysis of the high-temperature deformation of Ti–6Al–4V with a transformed microstructure, *Acta Mater.* 51 (18) (2003) 5613–5626.
- [21] Y. Chong, T. Bhattacharjee, R. Gholizadeh, J. Yi, N. Tsuji, Investigation on the hot deformation behaviors and globularization mechanisms of lamellar Ti–6Al–4V alloy within a wide range of deformation temperatures, *Materialia* 8 (2019) 100480.
- [22] N. Haghdadi, R. DeMott, P.L. Stephenson, X.Z. Liao, S.P. Ringer, S. Primig, Five-parameter characterization of intervariant boundaries in additively manufactured Ti–6Al–4V, *Mater. Des.* 196 (2020) 109177.
- [23] L. Wang, X.G. Fan, M. Zhan, X.Q. Jiang, X. Zeng, Y.F. Liang, H.J. Zheng, A.M. Zhao, The heterogeneous globularization related to crystal and geometrical orientation of two-phase titanium alloys with a colony microstructure, *Mater. Des.* 186 (2020) 108338.
- [24] T.R. Bieler, S.L. Semiatin, The origins of heterogeneous deformation during primary hot working of Ti–6Al–4V, *Int. J. Plast.* 18 (9) (2002) 1165–1189.